Talanta 193 (2019) 192–198

Contents lists available at ScienceDirect

Talanta

journal homepage: www.elsevier.com/locate/talanta

Detection of interstitial oxygen contents in Czochralski grown silicon crystals using internal calibration in laser-induced breakdown spectroscopy (LIBS)

Seyyed Ali Davari[a,c], Patrick A. Taylor[d], Robert W. Standley[e,1], Dibyendu Mukherjee[a,b,c,*]

[a] Department of Mechanical, Aerospace, & Biomedical Engineering, University of Tennessee, Knoxville, TN 37996, United States
[b] Department of Chemical & Biomolecular Engineering; University of Tennessee, Knoxville, TN 37996, United States
[c] Nano-BioMaterials Laboratory for Energy, Energetics & Environment (nbml-E3), University of Tennessee, Knoxville, TN 37996, United States
[d] ChemTrace, Quantum Global Technologies, LLC Company, Portland, OR, United States
[e] SunEdison Semiconductor Ltd., St. Peters, MO, United States

ARTICLE INFO

Keywords:
Laser-induced breakdown spectroscopy
Matrix effects
Internal standardizations
Interstitial oxygen
Czochralski silicon

ABSTRACT

We use an internal calibration approach in laser-induced breakdown spectroscopy (LIBS) for quantitative detection of dead load interstitial oxygen contents (O_i) in industrial-grade silicon (Si) crystal ingots. Si crystal samples were grown via Czochralski technique and supplied by SunEdison Semiconductor Ltd. with known O_i contents measured via gas fusion analysis (GFA) and Fourier transform infrared (FTIR) spectroscopy. The LIBS analyses reported here use and compare a direct approach based on the known oxygen atomic emission line at 777. 19 nm and an indirect approach based on an internal calibration technique using an emission line at 781 nm associated to Si I. Unlike the first direct approach, the latter exhibited much higher sensitivity, reliability and less error. In this approach, an internal calibration uses systematic variations in the 781 nm emission line in conjunction with observed changes in plasma excitation temperatures as a quantitative measure of changes in plasma conditions and laser-matter interactions due to varying O_i contents in the analyte matrix. Using this technique, we establish the detection limit of LIBS in measuring O_i in Si crystal ingots down to 8 ± 1 ppma level. The approach assists to overcome the limitations of common industrial techniques such as FTIR that cannot provide accurate quantitative measurements for heavily doped Si crystals and GFA that is significantly cumbersome to be an online technique. Our results establish LIBS at the forefront of alternative industrial analytical tools heretofore not considered for rapid, potential on-line monitoring of dead loads in commercial grade Si wafers during their growth processes.

1. Introduction

After more than 50 years, silicon is still the dominant semiconductor material in modern electronic devices, and the Czochralski (CZ) crystal growth process remains the most widely used method for producing the large diameter, single crystal starting material for semiconductor-grade silicon wafers. During the silicon CZ process, the fused silica (SiO_2) crucible containing the molten Si slowly dissolves, releasing oxygen into the molten Si. While most of this dissolved oxygen volatilizes from the Si melt in the form of SiO, a small fraction is transported by the melt flow to the growing crystal, and is incorporated as dissolved interstitial oxygen atoms, O_i, at a concentration of typically 2–20 ppm, atomic (ppma). The O_i concentration in the crystal can be controlled by adjusting a combination of several process parameters during the crystal growth. This dissolved O_i in the crystal has a profound influence on many aspects of the silicon wafers during device processing [1]. Beneficially, moderate levels of O_i impede the motion of dislocations [2], suppressing slip propagation in the Si wafer at high temperatures, and also provide a controlled oxygen precipitation that produces “internal gettering” [3] to trap metallic contaminants in the wafer bulk, away from the active device region. Too low an O_i concentration suppresses these benefits, while too high an O_i concentration can produce excessive oxygen precipitation that degrades wafer slip resistance [4] and can cause a variety of device failure issues [5]. Therefore, it is essential to have the appropriate metrology to monitor and control oxygen content in silicon wafers accurately.

Various techniques have been developed to quantify interstitial oxygen content in silicon wafers. The simplest, fastest, most precise and

* Corresponding author at: Department of Mechanical, Aerospace, & Biomedical Engineering, University of Tennessee, Knoxville, TN 37996, United States.
[1] SunEdison Semiconductor Ltd. is currently acquired by GlobalWafers Co. Ltd., St. Peters, MO, United States.

https://doi.org/10.1016/j.talanta.2018.09.078
Received 8 June 2018; Received in revised form 19 September 2018; Accepted 20 September 2018
Available online 26 September 2018
0039-9140/

most widely used technique is Fourier Transform Infrared spectroscopy (FTIR), in which the absorption peak of Si-O-Si asymmetric stretch mode at 1107 cm^{-1} is used to determine O_i content. However, FTIR cannot be used to measure O_i in heavily doped silicon wafers due to the strong free carrier absorption in the infrared in these materials. Gas fusion analysis (GFA) can be used for characterizing oxygen in silicon [6,7]. In GFA, a small piece of silicon is melted in a graphite crucible at temperatures between ~1500–1700 °C. The oxygen reacts with the graphite to form CO, which is transported via inert carrier gas over a catalyst that converts it to CO_2. The CO_2 is then analyzed and quantified by IR-absorption. While GFA is suitable for heavily doped wafers, it is known to be less sensitive when compared to FTIR techniques, and is considered as a destructive and time-consuming technique. Secondary ion mass spectroscopy (SIMS) has also been employed for characterizing oxygen content in heavily doped silicon wafers. However, like GFA, SIMS is a destructive, time-consuming technique with marginal precision. In addition, neither of these techniques can be implemented for on-line monitoring.

Laser Induced Breakdown Spectroscopy (LIBS) is considered as a relatively non-destructive spectrochemical characterization technique that can address the aforementioned issues in robust and yet reliable way. Typically, LIBS involves the collection and processing of spectral emissions emanating from the high-temperature, high-pressure plasma containing the analyte species of interest that is generated by focusing a pulsed laser on to the desired analyte sample [8]. In the past, LIBS has been employed for both quantitative and qualitative chemical analyses in highly diverse applications ranging from biomedical studies [9,10], thin films [11–13], nanomaterial analyses [14–16] to forensics [17] and explosive/energetic materials [18,19] in solid, gas and/or aerosol phase [20,21], and semiconductors [22–24].

In this study, we develop a robust and unique spectral methodology that enables the use of LIBS to quantify interstitial/dissolved O_i in commercial grade Si wafers. Here, our goal is to employ LIBS as an alternative analytical technique for potential on-line industrial monitoring in future for the commercial Si manufacturing sector. The Si crystal samples used here for our analytical study were provided by SunEdison Semiconductor Ltd. as part of a research grant to support their R&D efforts in these directions. As pilot test efforts, SunEdsion had provided us with Si wafers carrying known interstitial O_i concentrations varying between zero (in Float Zone silicon) up to ~17 ppma. These concentrations are pre-determined in SunEdison Semiconductor's research facilities using FTIR and GFA techniques. The research results presented here led to the development of a LIBS calibration curve that indicates clear correlations between the SunEdison provided FTIR results, the well-known oxygen (777.19 nm) atomic emission line and a less employed Si (781 nm) atomic emission line. Such measurements, not carried out heretofore, allow for a highly specific and indirect instrument calibration for LIBS that can potentially lead to its commercial applications for high-sensitivity detection of O_i in industrial grade Si wafers.

2. Experimental details

2.1. LIBS Set-up

Fig. 1 illustrates the experimental set-up. The laser-induced plasma is generated on the sample target surface using a Q-switched Nd-YAG laser of nominal wavelength 1064 nm operating at 200 mJ/pulse, and a pulse width of 8 ns (Make: Insight Model: 122551-R). The laser with repetition rate 10 Hz is focused with a 25 mm diameter fused silica lens (focal length = 35 mm). The spot size on the sample is set by the in-built instrument software to 75 μm diameter, which typically creates millimeter-sized plasma. To improve the statistical average of the signal intensity for each analyte of interest, 50 accumulative shots at each spot are collected after 20 cleaning shots. The 50 accumulated shots were averaged into 1 spectrum and used for signal calculations. For each

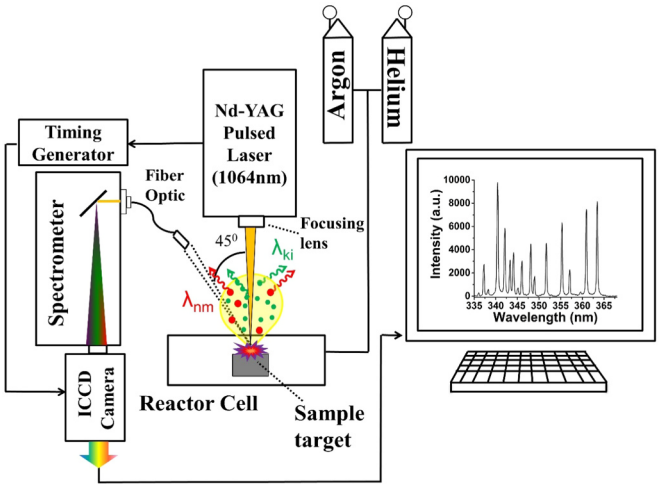

Fig. 1. Schematic of LIBS experimental set-up used in this study.

sample, more than 50 such spots are analyzed and averaged. The samples are placed in a specific chamber designed for this study. An inlet valve allows various gases to be purged in the chamber, and an exhaust valve connected to a vacuum pump can deplete the buffer gas inside the chamber.

To optimize the intensity from the plasma volume a fiber optic port is mounted at 45° collection angle and collects the plasma emissions (Fig. 1). The focused light is transmitted to a Czerny-Turner spectrometer (Make: Andor Technology; Model: Shamrock - SR-303i-A) with 1200 grooves/mm grating (resolution of 0.1 nm at 500 nm) and a nominal dispersion of 2.58 nm/mm. The slit width is fixed at 95 μm for all experiments carried out here in order to have the optimum spectral line intensity and resolution. The spectrometer is calibrated against Hg emission at 253.65 nm using Mercury lamp (Make: Ocean Optics). A time-gated intensified charge-coupled device (ICCD) detector array (1024 × 1024 CCD) (Make: Andor Technology; Model: DH334T-18U-E3) detects the spectral lines at the spectrometer exit focal plane. The time gating is synchronized with the laser Q-switch through an in-built timing generator in the ICCD camera set-up.

The polished silicon samples were characterized using FTIR in SunEdison Semiconductor facilities and then cut to approximately 2 × 1 × 1 cm^3 pieces prior to be tested using LIBS at University of Tennessee. The 1107 cm^{-1} IR absorption peak height was converted to Oi concentration using the ASTM 121–80 (“New ASTM”) calibration factor. Moreover, standard commercial Si wafers (make: University Wafer) of thickness 500 μm were used as negative controls to verify specific Si lines and compare to SunEdison polished silicon samples. The samples were tested using LIBS in an in-house built reactor cell while both helium (6 lpm) and argon (2 lpm) were purged into the cell as the buffer gas. The choice of flow rates has been discussed earlier [12]. LIBS measurements are subject to error if oxygen is present in any form other than interstitial oxygen. Therefore, in order to eliminate any oxygen signal from the native oxide layer on top of silicon wafer they are dipped into 10% hydrofluoric (HF) acid for 10 min. To improve the statistical analysis 50 spots and 50 shots at each spot were collected for each sample. For each concentration 5–6 different samples were tested to improve the statistical average.

2.2. LIBS methodology

The atomic emission lines were selected from the NIST Atomic Energy Levels Data Center [25] according to their relative lines transition probabilities and strength. To achieve optimum accuracy in the results, the optimal gate delays are determined based on the variations of signal-to-noise ratios (SNR) as a function of gate delays for the

respective elemental species. The SNR is calculated by measuring the peak signal value at the specific wavelength of interest for a spectral line divided by the noise of the spectra. The noise is defined as the root mean square over the baseline (~ over 40 pixel) adjacent to the analyte peak. The optimum SNR is used as the effective emission (I_{em}) and the Maxwell-Boltzmann relation is used for calculating the plasma temperature using various argon transition lines:

$$N_k = N\frac{g_k e^{\frac{-E_k}{k_B T_{exc}}}}{U(T_{exc})} \quad (1)$$

Considering the emission flux captured by the ICCD camera:

$$I_{em} = \frac{hc}{\lambda_{ki}} N_k A_{ki} \quad (2)$$

Substituting N_k from Eqs. (1) to (2), we obtain:

$$\ln\left(\frac{I_{em}\lambda_{ki}}{g_k A_{ki}}\right) = -\frac{E_k}{k_B T_{exc}} + \ln\left(\frac{Nhc}{U(T_{exc})}\right) \quad (3)$$

where N_k, A_{ki}, λ_{ki}, g_k are atomic number densities at the higher energy state, Einstein's transition probability, emitted wavelength, and statistical weights for the higher (k) energy state respectively for the specific atomic transition of interest. E_k represents the energy of higher (k) state, and T_{exc} is the plasma excitation temperature at the optimal gate delays. Boltzmann and Planck's constant are indicated by k_B (1.38064×10^{-23} m^2 kg/s^2 K) and h (6.62607×10^{-34} m^2kg/s) respectively, and c (3×10^8 m/s) is the speed of light in vacuum. The plasma excitation temperatures (T_{exc}, K) are determined from the slope of the fit to the linear Boltzmann plot of $\ln(I_{em}\lambda_{ki}/g_k A_{ki})$ as a function of normalized upper energy levels (E_k/k_B) for multiple strong argon lines with sufficiently widespread upper energy levels under local thermodynamics equilibrium (LTE) assumption.

3. Results and discussion

The known amounts of O_i in the Si crystal samples, as provided by SunEdison Semiconductor and tabulated in Table 1, were measured at the SunEdison research facilities using standard FTIR and GFA measurements. Our initial approach for detecting dissolved O_i species in the Si samples relied on the direct analysis of the spectral signature for well-known triplet O I at 777 nm. Specifically, we have chosen O I (777.19 nm) atomic emission line due to greater relative intensity. This was initiated with the determination of optimal gate delay from the temporal evolution of the SNR for the O I spectral emissions as indicated in Fig. 2. It was observed that the maximum spectral SNR for O I (777.19 nm) occurred at 3.5 μs gate delay. In this approach, it was essential to eliminate any undesired oxygen signal arising from the background. To this end, two major sources of undesired background oxygen could be immediately identified, namely native oxide layer sample surface and oxygen in the background buffer. To eliminate the first source, the samples are dipped into 10% HF for 10 min. To address the second source, the sample chamber is filled with a buffer gas mixture of 6 lpm He and 2 lpm Ar while keeping the exhaust valve closed and subsequently, vacuuming with the inlet valve being closed. This purge cycle process is repeated multiple times to deplete the system of any residual background oxygen. Fig. 3 shows the variation of O I (777.19 nm) emission as a function of number of purge cycle for the Si wafer sample with 16.90 ppm O_i contents. It can be observed that the O I (777.19 nm) emission diminishes to an almost constant value after approximately ~ 10 purge cycles. Therefore, the numbers of purge cycle is fixed as 10 for all the experiments reported here. In this straightforward spectroscopic approach, ideally we should be able to calibrate the SNR for O I (777.19 nm) emission as a function of the O_i contents in the samples provided the specific O I signals are distinguishable from the background noise. However, the extremely low O_i concentrations in the supplied Si crystal wafers (< 17 ppm) resulted in a relatively poor detection of O_i from the background oxygen and the construction of a calibration curve (Fig. 4) with low sensitivity. As it can be observed, the slope of the calibration curve (sensitivity) and the error bars (standard deviations) are significantly poor, which made the direct LIBS quantitative approach unsuitable for the accuracy level required for the specific industrial application here.

Table 1
Interstitial oxygen concentration (O_i) is silicon ingots measured using FTIR and GFA in SunEdison's research facilities.

Sample	Sample 1	Sample 2	Sample 3	Sample 4	Sample 5
Interstitial oxygen content (O_i)	FZ (0 ppm)	9.10 ppm	10.99 p.m.	14.25 ppm	16.90 ppm

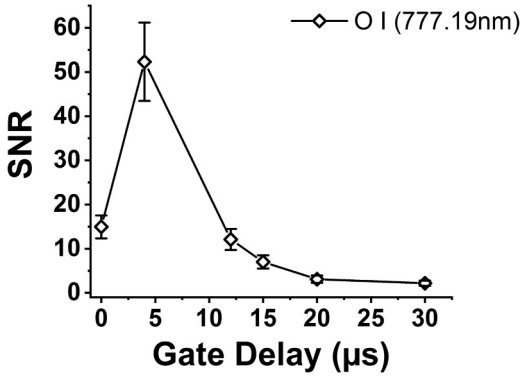

Fig. 2. Variation of signal-to-noise ratio (SNR) for O I (777.19 nm) emission line as a function of gate delays. The optimum gate delay was determined as 3.5 μs.

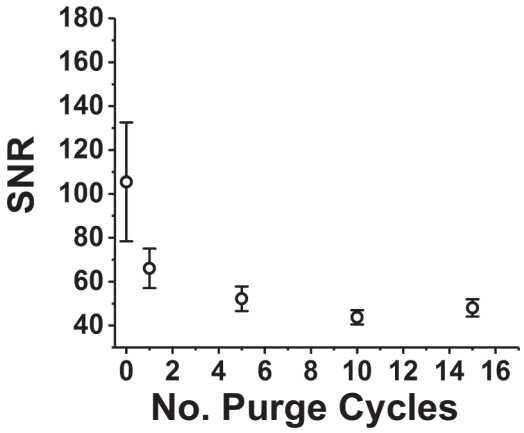

Fig. 3. Variation in SNR of OI (777. 19 nm) emission line as a function of the number of purge cycles.

Having faced with inadequate sensitivity, a careful and detailed analyses of the LIBS spectra obtained from the various Si wafer samples led to our observation of a distinct spectral peak occurring at 781 nm next to the known O I (777.19 nm) line (Fig. 5). It needs to be mentioned here that a thorough search of the NIST spectral database could not identify the source of this emission line among either the atomic or ionic lines. During an extensive literature review, we found only one paper that had briefly discussed about this emission line in Si samples and had tentatively ascribed it to an atomic emission line for Si [26]. But, the lack of any detailed information on the spectral parameters for this line still made it difficult for us to resort to any direct quantitative LIBS analysis using this emission line. It needs to be reiterated here that all our LIBS measurements were carried out in a buffer gas containing

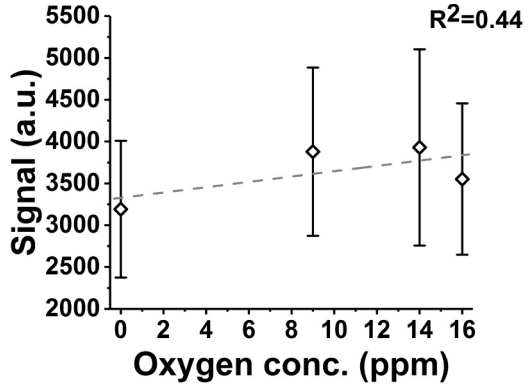

Fig. 4. Calibration curve for direct quantitative LIBS analysis from O I (777.19 nm) emission line for commercial Si crystal wafers with known interstitial oxygen (O_i) concentrations (ppm).

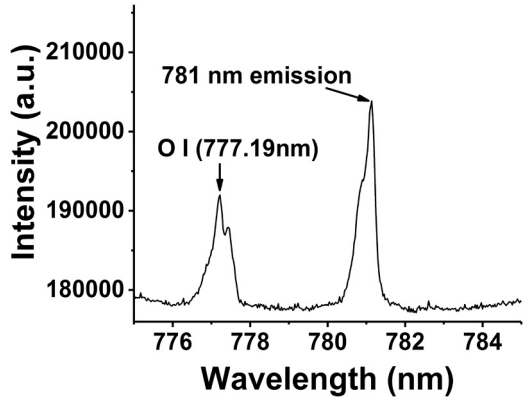

Fig. 5. Spectral emission signature for O I (777.19 nm) and the observed emission line at 781 nm.

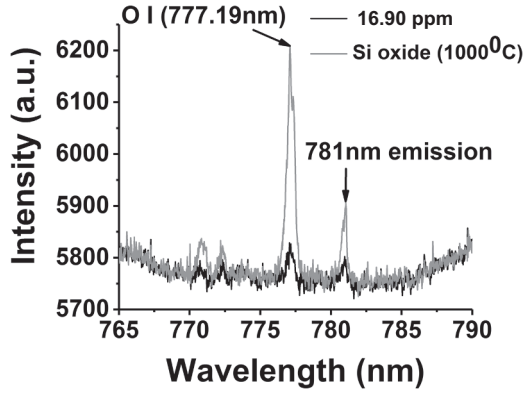

Fig. 6. Spectral emission signatures for O I (777.19 nm) and 781 nm lines as collected from commercial Si crystal wafer with 16.90 ppm O_i concentrations and thin SiO_2 layer (synthesized from thermal oxidation at 1000 °C) in the presence of N_2 as the buffer gas.

He, Ar and minor background O. Hence on careful consideration, the lack of any other supporting evidence for the particular Si line prompted us to further confirm and verify that this line was not emanated from other Ar, He atomic emissions and/or, some forms of SiO_x molecular emissions from within the plasma. To eliminate these possibilities, firstly we specifically created thin SiO_2 layer on top of standard commercial (Make: University Wafer) Si wafers (not the SunEdison supplied Si Crystal samples) via direct thermal oxidation in an oven at exceedingly high temperatures (above 900 °C). The rationale here was to provide a negative control that would confirm that the LIBS emission for the 781 nm line: 1) is not unique to the Si crystal samples provided by SunEdison Semiconductor Ltd only, 2) does not emanate from any background species, and finally, 3) does not change with excess amount of oxygen. To this end, we carried out LIBS measurements on these SiO_2 film coated commercial Si wafers inside the chamber filled with nitrogen as the buffer gas. The LIBS spectral signature from Fig. 6 indicates that the 781 nm peak is still detectible from the SunEdison samples and commercial Si wafers coated with SiO_2 thin layer (for ~ 1000 °C thermal oxidation) in the presence of background N_2 and the absence of He and Ar. Therefore, it can be concluded that the 781 nm emission is not a contribution of atomic lines from any of the background He or Ar, molecular emissions and/or, is not unique to any specific type of the Si samples used. Thus, we concluded that the 781 nm emission line is specific to either atomic or molecular emissions originating from one of the species of Si, O and/or some molecular intermediates of SiO_x formed in the plasma. Thereby, in our systematic effort to analyze the relation of the 781 nm line to O and/or, Si based species in the plasma, we carried out a series of LIBS experiments on thin film SiO_2 layers of different thicknesses created on the commercial-grade Si wafers via thermal oxidation at different oven temperatures (900° –1050 °C). The rationale behind this control experiment was that if the 781 nm emission line is related to O or any form of molecular SiO_x species formed in the plasma, then the emission signal should vary for different oxide film thicknesses on the samples. To this end, Fig. 7 illustrates the LIBS spectra collected from the standard commercial Si wafers carrying oxide film layers of various thicknesses. It is clearly observed that while the O I (777.19 nm) emission line intensity increases with increasing amount of O (as expected due to increasing oxide layer thicknesses of ~ 0–189 nm), the 781 nm emission line indicates no change in its intensity due to the varying SiO_2 thickness layers. The fact that the 781 nm line exists in all of the SiO_2 thin film samples without indicating any variations in their respective strengths leads to our conclusion that this emission is not related to any O bearing species or any form of SiO_x species but, is purely related to the bulk Si present in all the samples as also conjectured in the earlier literature [26]. Here we would to like mention that upon careful consideration of all the possible atomic emission lines for Si and based on a valuable comment from one of the paper's reviewers during the review of this article, a plausible explanation for the origin of the 781 nm emission is that it arises from the second order peak for the well-known strong Si I line at 390.55 nm. To our advantage, the proximity of the 781 nm emission to the oxygen emission at 777.2 nm made the use of the 781 nm line more conducive for us to capture both the silicon and oxygen emissions with the same laser shot in the same window.

Now, we proceeded to use this specific emission (I_{si}) and O I (777.19 nm) emissions (I_O) to construct a new calibration curve in Fig. 8 using the normalized signal intensities for I_{si}/I_O as a function of O

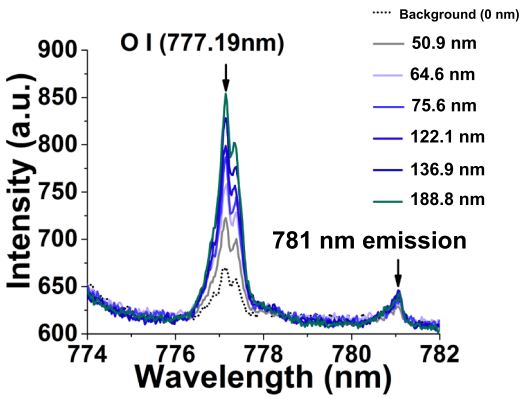

Fig. 7. Variations of O I (777.19 nm) and 781 nm emission lines with SiO_2 thickness changes on thermally oxidized Si wafers indicating no variation in the 781 nm emission due to changes in oxygen contents.

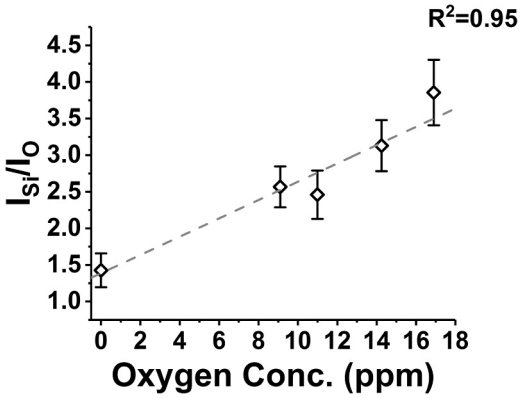

Fig. 8. Calibration curve constructed from matrix-assisted LIBS data analyses based on O I (777.19 nm) and 781 nm emissions indicating significant sensitivity improvement for the detection of Oi contents (ppm).

Table 2
Atomic spectral database [25] for different argon atomic emission lines used for the plasma excitation temperature calculations at 3.5 μs for the different Si samples.

Species	Wavelength, λ_{ki} (nm)	Transition probability, A_{ki} (10^5 1/s)	Upper energy level E_k (eV)	Lower energy level E_i (eV)	g_k	g_i
Ar I	415.859	14	14.5289	11.5484	5	5
Ar I	420.068	9.67	14.4991	11.5484	7	5
Ar I	425.936	39.8	14.7381	11.8281	1	3
Ar I	427.217	7.97	14.5249	11.6236	3	3
Ar I	433.356	5.68	14.6883	11.8281	5	3
Ar I	696.543	63.9	13.3279	11.5484	3	5
Ar I	706.722	38	13.3022	11.5484	5	5

concentrations (ppma) for the SunEdison supplied samples of known O_i contents. One can clearly observe that the sensitivity for the calibration improved considerably upon using the normalized 781 nm emission line intensity as compared to our earlier calibration solely based on the O I (777.19 nm) emission line (compare to Fig. 4). It is noted that the slope of the calibration increased while the uncertainty of the data points decreased significantly. Here, we attribute the improvement in the calibration to matrix-assisted plasma physics associated with an increase in the sensitivity of capturing plasma condition variations due to inherent alterations in the laser-induced plasma-matter coupling arising from the varied O_i contents in the different Si crystal samples. Specifically, to further confirm these matrix-assisted plasma condition variations with O_i concentrations in the Si samples, plasma excitation temperatures ($T_{exc,}$ K) are calculated from normalized linear Boltzmann plots constructed for various well-known Ar transition lines (see Table 2 for the line properties used).

Fig. 9 illustrates the representative strong Ar emission lines at different spectral windows collected for an example Si sample carrying [Oi] 16.90 ppm and subsequently, used for all the T_{exc} calculations here. Fig. 10 illustrates the linear Boltzmann plots for the different representative Si wafer samples with carrying [O_i] concentrations of 0 ppm (Float Zone), 9.10 ppm, 10.99 ppm, 14.25 ppm, and 16.90 ppm. As reported in Table 3, one can clearly see that the plasma excitation temperatures indicate a systematic increase (T_{exc} =;10,652.91 ± 928.32 K, 10,700.40 ± 1031.15 K, 13,523.59 ± 1778.67, 14,332.89 ± 2135.16 K, and 15,217.71 ± 2379.02 K) as the O_i concentration increases in the different Si samples. Thus, as plotted in Fig. 11, the T_{exc} from the LIBS analyses on different O_i containing Si crystal samples indicate two distinct regions - an initial plateau (between Float Zone and 9.10 ppm sample) and a linear part (between 9.10–16.90 ppm samples). In past studies on Si crystals, Youssef et al. had shown that the physical and mechanical properties of Si wafers can change drastically with increasing interstitial O_i concentrations [27]. Such observations can readily explain our observed results from the matrix-assisted LIBS analyses indicating that an increase in the O_i concentrations in our SunEdison supplied Si crystal wafers also alters the laser ablation mechanism, laser-matter coupling and the plasma conditions generated by the samples. In fact, the increasing plasma excitation temperatures ($T_{exc,}$ K) with increasing O_i concentrations in the Float Zone (0 ppm) to 16.90 ppm samples in Fig.11 clearly corroborates this matrix-driven plasma physics alteration for in the Si crystal samples under study here. Also, it needs to be pointed out that the temperature calibration curve in Fig. 11 does not indicate significant difference between the Float Zone and 9.10 ppm sample. Finally, using the fluctuations in the normalized intensities (σ) and the slope of the calibration curve (S) in Fig. 8:

$$\mathrm{LOD} = \frac{3\sigma}{S} \tag{4}$$

the limit of detection (LOD) is determined for the interstitial oxygen in silicon wafers as 8 ± 1 ppma. The precision in this study is approximately 16% RSD. It is worth mentioning that the current precision needs further improvement before the methodology actually is implemented for on-line measurement. For the readers' references, Table S1 in the supplementary information summarizes the interstitial oxygen concentrations as obtained by LIBS calibration curve and reported by FTIR/GFA.

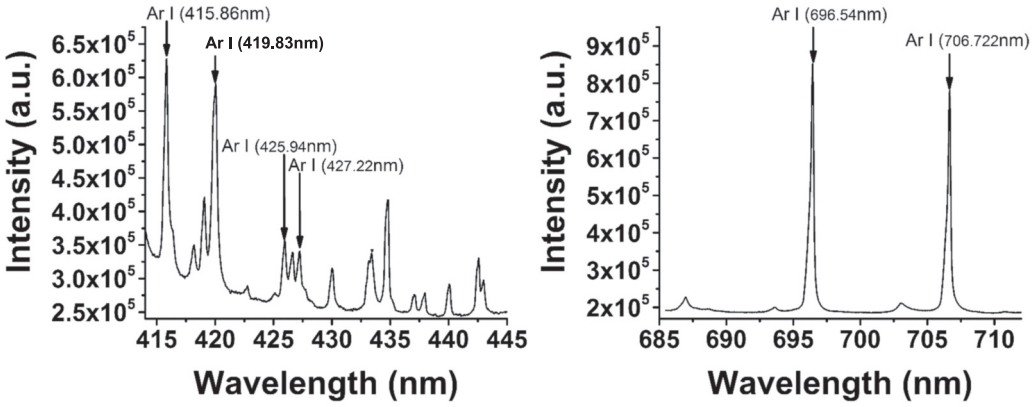

Fig. 9. Spectral emission signatures of various argon transition lines used to extract plasma excitation temperature.

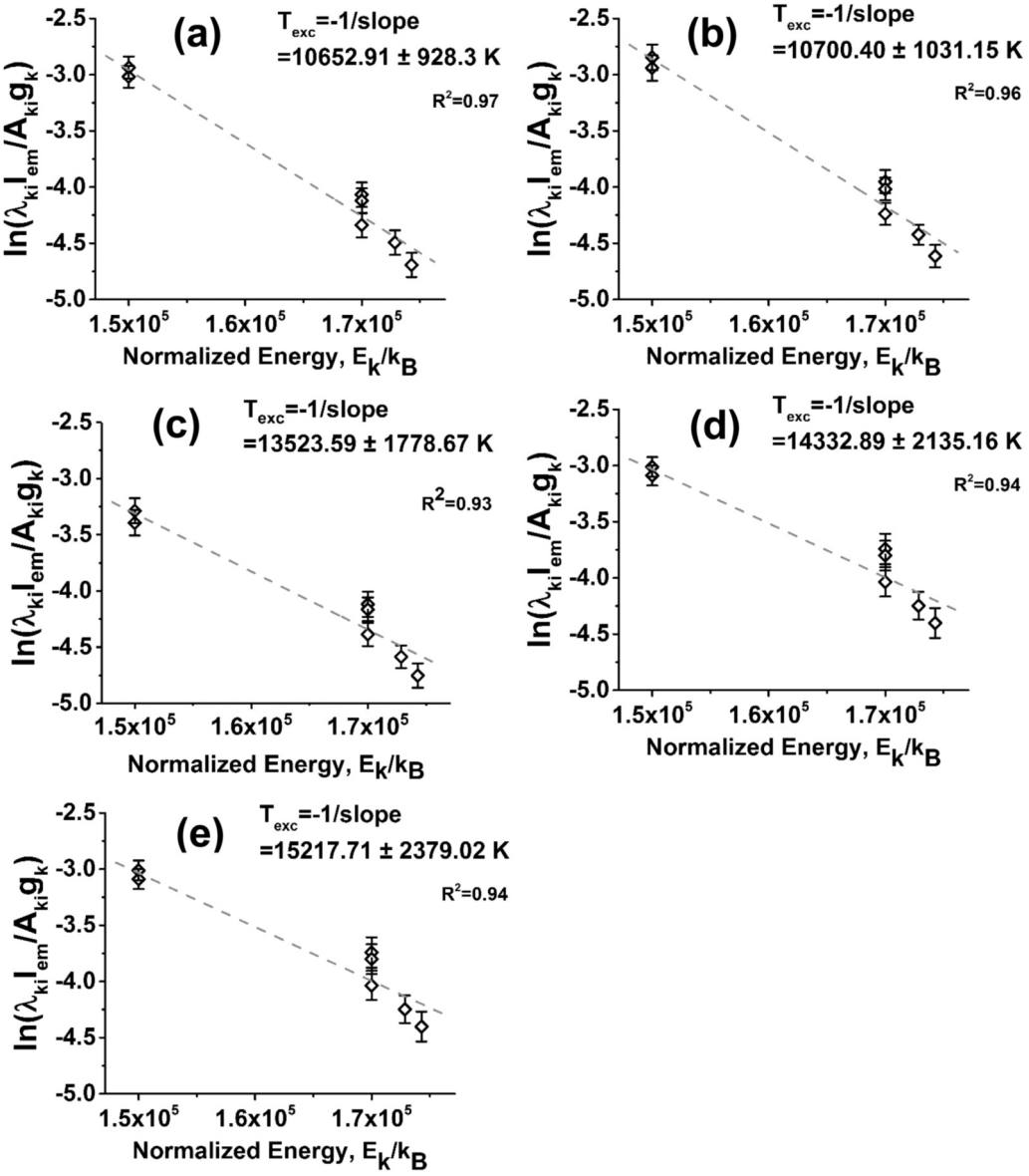

Fig. 10. Normalized linear Boltzmann plots constructed based on Ar transitions lines collected for various Si wafer samples with different O_i concentrations of: (a) 0 ppm (Float Zone), (b) 9.10 ppm, (c) 10.99 ppm, (d) 14.25 ppm, and (e) 16.90 ppm.

Table 3
Plasma excitation temperatures (T_{exc}) calculated from linear Boltzmann plots using Ar transition lines for the various Si samples with different interstitial oxygen contents, O_i.

Sample	FZ (0 ppm)	9.10 ppm	10.99 p.m.	14.25 ppm	16.90 ppm
Temperature (K)	10,652.91 ± 928.32	10,700.40 ± 1031.15	13,523.59 ± 1778.67	14,332.89 ± 2135.16	15,217.71 ± 2379.02

4. Conclusion

Laser-induced breakdown spectroscopy (LIBS) has been employed to determine the interstitial oxygen in commercial silicon wafers quantitatively. The results indicated that using oxygen emission O I (777.19 nm) provide poor sensitivity and calibration. An emission at 781 nm was observed that was correlated to silicon emission. Using both 781 nm and O I (777.19 nm), we were able to improve the calibration significantly. The plasma excitation temperature illustrated a systematic change as the interstitial oxygen content varies in samples. The variation in plasma temperature was related to change in amount of ablated sample due to drastic difference in hardness of the samples. This result shows the potential and sensitivity of LIBS to variations in ablated mass and plasma condition. The results of this study introduce LIBS as an effective quantitative analytical tool that can address the industrial needs for the semiconductor manufacturing sector.

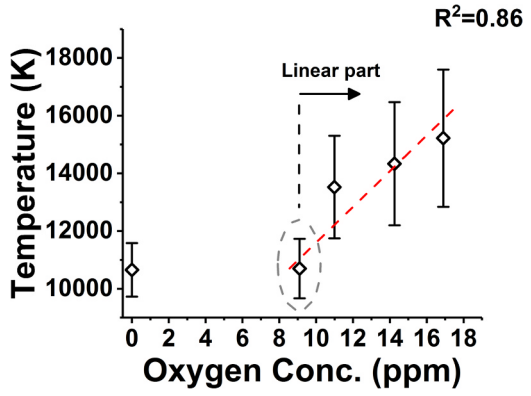

Fig. 11. Systematic variations in plasma excitation temperatures ($T_{exc,}$ K) for LIBS spectra collected over various Si crystal samples with increasing interstitial oxygen concentrations (ppm).

Acknowledgement

The authors would like to thank SunEdison Semiconductor Ltd. for supporting this project financially. Moreover, the authors would like to thank one of the reviewers for providing valuable suggestion regarding the source of emission at 781 nm.

Appendix A. Supporting information

Supplementary data associated with this article can be found in the online version at doi:10.1016/j.talanta.2018.09.078.

References

[1] F. Shimura, Oxygen in Silicon 42 Academic Press, 1994.
[2] K. Sumino, M. Imai, Interaction of dislocations with impurities in silicon-crystals studied by insitu X-ray topography, Philos. Mag. A 47 (5) (1983) 753–766.
[3] G.A. Rozgonyi, R.P. Deysher, C.W. Pearce, Identification, annihilation, and suppression of nucleation sites responsible for silicon epitaxial stacking-faults, J. Electrochem. Soc. 123 (12) (1976) 1910–1915.
[4] I. Yonenaga, K. Sumino, K. Hoshi, Mechanical strength of silicon-crystals as a function of the oxygen concentration, J. Appl. Phys. 56 (8) (1984) 2346–2350.
[5] L. Jastrzebski, R. Soydan, J. Mcginn, et al., A comparison of internal gettering during bipolar, cmos, and ccd (high, medium, low-temperature) processes, J. Electrochem. Soc. 134 (4) (1987) 1018–1025.
[6] H. Walitzki, H. Rath, J. Reffle, S. Pahlke, M. Blatte, Control of oxygen and precipitation behaviour of heavily doped silicon substrate materials, Semicond. Silicon (1986) 86.
[7] R.W. Shaw, R. Bredeweg, P. Rossetto, Gas fusion analysis of oxygen in silicon - separation of components, J. Electrochem. Soc. 138 (2) (1991) 582–585.
[8] L.J. Radziemski, D.A. Cremers, Spectrochemical analysis using laser plasma excitation, Laser-Induc. Plasmas Appl. (1989).
[9] V.A. Riberdy, C.J. Frederickson, S.J. Rehse, Determination of the zinc concentration in human fingernails using laser-induced breakdown spectroscopy, Appl. Spectrosc. 71 (4) (2017) 567–582.
[10] S.A. Davari, S. Masjedi, Z. Ferdous, D. Mukherjee, In-vitro analysis of early calcification in aortic valvular interstitial cells using Laser-Induced Breakdown Spectroscopy (LIBS), J. Biophotonics. 11 (1) (2018).
[11] C.K. Kim, S.H. Lee, J.H. In, H.J. Lee, S. Jeong, Depth profiling analysis of CuIn1-xGaxSe2 absorber layer by laser induced breakdown spectroscopy in atmospheric conditions, Opt. Express 21 (22) (2013) A1018–A1027.
[12] S.A. Davari, S. Hu, R. Pamu, D. Mukherjee, Calibration-free quantitative analysis of thin-film oxide layers in semiconductors using laser induced breakdown spectroscopy (LIBS), J. Anal. At. Spectrom. 32 (7) (2017) 1378–1387.
[13] Ş. Yalçın, S. Örer, R. Turan, 2-D analysis of Ge implanted SiO2 surfaces by laser-induced breakdown spectroscopy, Spectrochim. Acta Part B At. Spectrosc. 63 (10) (2008) 1130–1138.
[14] S. Hu, E.L. Ribeiro, S.A. Davari, M.K. Tian, D. Mukherjee, B. Khomami, Hybrid nanocomposites of nanostructured Co3O4 interfaced with reduced/nitrogen-doped graphene oxides for selective improvements in electrocatalytic and/or supercapacitive properties, RSC Adv. 7 (53) (2017) 33166–33176.
[15] S.A. Davari, S. Hu, E.L. Ribeiro, D. Mukherjee, Rapid elemental composition analysis of intermetallic ternary nanoalloys using calibration-free quantitative laser induced breakdown spectroscopy (LIBS), MRS Adv. 2 (55) (2017) 3371–3376.
[16] S.A. Davari, S. Hu, D. Mukherjee, Calibration-free quantitative analysis of elemental ratios in intermetallic nanoalloys and nanocomposites using laser induced breakdown spectroscopy (LIBS), Talanta 164 (2017) 330–340.
[17] E.M. Rodriguez-Celis, I.B. Gornushkin, U.M. Heitmann, et al., Laser induced breakdown spectroscopy as a tool for discrimination of glass for forensic applications, Anal. Bioanal. Chem. 391 (5) (2008) 1961–1968.
[18] M. Weidman, M. Baudelet, S. Palanco, M. Sigman, P.J. Dagdigian, M. Richardson, Nd:YAG-CO_2 double-pulse laser induced breakdown spectroscopy of organic films, Opt. Express 18 (1) (2010) 259–266.
[19] J.L. Gottfried, F.C. De Lucia, C.A. Munson, A.W. Miziolek, Laser-induced breakdown spectroscopy for detection of explosives residues: a review of recent advances, challenges, and future prospects, Anal. Bioanal. Chem. 395 (2) (2009) 283–300.
[20] D. Mukherjee, A. Rai, M.R. Zachariah, Quantitative laser-induced breakdown spectroscopy for aerosols via internal calibration: application to the oxidative coating of aluminum nanoparticles, J. Aerosol Sci. 37 (6) (2006) 677–695.
[21] D.W. Hahn, M.M. Lunden, Detection and analysis of aerosol particles by laser-induced breakdown spectroscopy, Aerosol Sci. Tech. 33 (1–2) (2000) 30–48.
[22] X.L. Mao, X.Z. Zeng, S.B. Wen, R.E. Russo, Time-resolved plasma properties for double pulsed laser-induced breakdown spectroscopy of silicon, Spectrochim. Acta B 60 (7–8) (2005) 960–967.
[23] M. Milan, P. Lucena, L.M. Cabalin, J.J. Laserna, Depth profiling of phosphorus in photonic-grade silicon using laser-induced breakdown spectrometry, Appl. Spectrosc. 52 (3) (1998) 444–448.
[24] Z.G. Ji, J.H. Xi, Q.N. Mao, Determination of oxygen concentration in heavily doped silicon wafer by laser induced breakdown spectroscopy, J. Inorg. Mater. 25 (8) (2010) 893–896.
[25] A. Kramida, Ralchenko, Yu., Reader, J. and NIST ASD Team. NIST Atomic Spectra Database (version 5.3). [[Online]]; 〈http://physics.nist.gov/asd〉.
[26] T. Makimura, K. Murakami, Dynamics of silicon plume generated by laser ablation and its chemical reaction, Appl. Surf. Sci. 96–8 (1996) 242–250.
[27] K. Youssef, M. Shi, C. Radue, E. Good, G. Rozgonyi, Effect of oxygen and associated residual stresses on the mechanical properties of high growth rate Czochralski silicon, J. Appl. Phys. 113 (13) (2013).